Evaluation of fractures in a concrete slab by means of laser-spot thermography

Agnese Scalbi

IAC "M. Picone" - CNR, Via Madonna del Piano 10, 50019 Sesto Fiorentino, Italy

Roberto Olmi

IFAC - CNR, Via Madonna del Piano 10, 50019 Sesto Fiorentino, Italy

Gabriele Inglese

IAC "M. Picone" - CNR, Via Madonna del Piano 10, 50019 Sesto Fiorentino, Italy

Abstract

The presence of cracks is a determining factor for the deterioration of reinforced concrete structures. Laser Spot Thermography (LST) is a fast and contactless technique for cracks identification. A computational procedure to characterize the crack depth by means of LST is presented here. We propose a heuristic form of the temperature at the concrete slab surface from which we derive a relation (called β-tool) between the thermal gap across the crack and the unknown depth of the damage. In this way, by means of a fast survey, it is possible to distinguish between shallow and deep fractures (more than 15mm deep), for which further specific analysis will be needed.

Keywords: Laser-spot thermography, thermography, inverse problems, nondestructive evaluation, concrete fracture, diagnostics

1. Introduction

This note deals with the problem of evaluating the size of fractures that may appear on the surface of reinforced concrete structures. Noticeable fractures and invisible micro-cracks reduce the performance of the material so that their early detection is crucial as pointed out in some introductory technical reports [1] [2] and in recent state-of-the-art [3].

Fractures in concrete have many different origins: drying shrinkage, thermal contraction, applied loads, freeze-thaw cycles, sulfate attack, alkali-aggregate reactivity, corrosion of rebar ([4], [5] [6], [7], [8] to cite few amongst thousands). Hence, their evaluation requires the solution of specific inverse problems according to the choice of appropriate mathematical models and detection techinques

Nomenclature:

Geometrical Parameters	
Ω	undamaged domain
Ω_σ	ideal cracked domain
Ω_ϵ	real cracked domain
C_ϵ	eal crack
b	crack depth
x_0	crack position relative to laser spot
σ	ideal crack
ϵ	crack half-width
Physical Parameters	
T	temperature
U^0	initial temperature
u	temperature increase $T - U_0$
u_0	background temperature increase in Ω
u^ϵ	temperature increase in $\Omega_epsilon$
u_c^ϵ	temperature increase in $C_epsilon$
u_σ	temperature increase in Ω_sigma
ρ	slab density
C	slab specific heat
κ	slab thermal conductivity
ρ_c	air density
C_c	air specific heat
κ_c	air thermal conductivity
α	slab thermal diffusivity
H	heat transfer coefficient
H_{eff}	effective heat transfer coefficient
ϕ_L	maximum power of the laser source
δ_L	standard deviation of the laser source
Acronyms	
LST	Laser Spot Thermography
IBVP	Initial Boundary Value Problem
FEM	Finite Elements Method

(see for example [9], [10], [11], [12] about numerical-geometrical models and [13], [14], [15], [16], [18], [19], [20] about detection methods).

Suppose that a fracture σ has been revealed on the surface of an artifact. Our goal is to evaluate, by means of Active Infrared Thermography (AIT: see [16]), hidden average characters of σ like depth, width and shape inside the specimen. AIT is a contactless, fast and non-invasive technique successful in nondestructive evaluation of shallow defects. When the depth of the defect is much larger than its width (as in the case of cracks) Laser Spot Thermography (LST), a special case of AIT, is required.

LST is well known to give good results in crack evaluation. A laser provides a localized heating spot so that heat flows isotropically into the undamaged artifact giving rise to half-spherical temperature contour levels. A circular spot, centered in a point P_L close to the fracture σ, is heated with a laser for a time interval t_L lasting from one second to one minute approximately (see Figure 1). We consider cracks whose time evolution is negligible in an interval $(0, t_L)$. For this reason σ is assumed constant in t. The study of thermal anomalies due to the presence of a defect, gives us the possibility to evaluate width and depth of the fracture. Some qualitative information about the internal shape of σ can be obtained also.

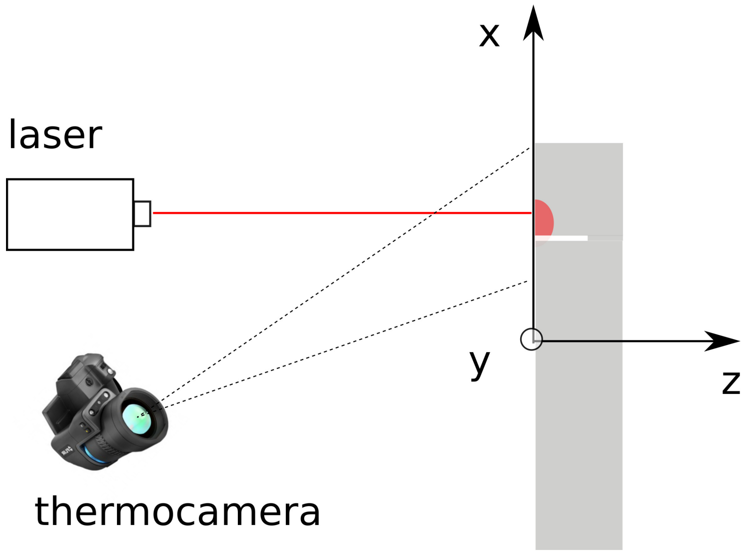

Figure 1: Schematic of the laser-spot thermography setup

In this paper, the numerical analysis of heat propagation in presence of a fracture in concrete elements is carried out by means of a 2D FEM simulation. The mathematical model is defined in section 3. The presence of a perpendicular air-filled (i.e. almost insulating) crack, close to the heated spot, perturbs the shape of temperature contour levels (section 4). A quantitative analysis of the perturbation leads to the evaluation of the crack. In our framework, the low thermal conductivity brings to long heating and observation times so that stationary models are useless. Furthermore, fractures are wider, deeper and more jagged compared to metal components.

Since thermography is known to be effective in the detection of subsurface anomalies, a method based on LST is naturally focused to the early detection of fractures that arise on the surface and grow up inside the specimen. The temperature on the damaged surface is expressed in terms of the background temperature suitably weighted (section 4.2). This leads to a fast and reliable method for the evaluation of the main properties of a real fracture in a limited but significant depth range. A fracture out of this range will be reported as potentially dangerous so further analysis with a different method will be required.

Simulations and results with real data are reported in sections 6.2 and 7.

2. Geometry of the problem. Ideal and physical cracks.

An ideal, normal *crack* is a bended strip orthogonal to the lower face of a parallelepiped-shaped specimen. A *physical normal crack* (or *fracture*) is a thin neighborhood of the (ideal) crack. The connection between ideal and physical cracks, in the context of Initial Boundary Value Problems for the heat equation, is studied in section 4.1.

Although the geometrical figure that represents the concrete slab at hand is clearly a parallelepiped $\Omega_{a,R} = (-R, R) \times (-R, R) \times (0, a)$ with $0 < a < R$, we assume in what follows that our specimen is the half-space $\Omega = \{z \geq 0\}$. Since we deal with short-lasting experiments and simulations, it is easy to realize that these assumptions are not restrictive as long as we have in mind materials characterized by low diffusivity. A quantitative analysis of this fact is in [17] section 2.1.

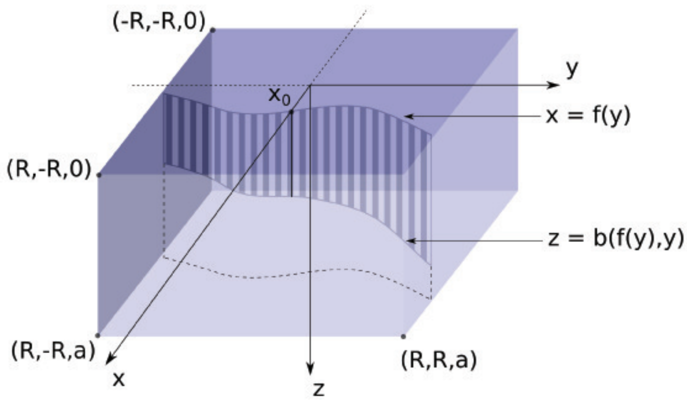

Figure 2: Geometry of the problem.

In the geometrical framework in which Ω is the specimen, a crack is the infinte strip shown in Figure 2. A formal definition of σ is:

$$\sigma = \{(x, y, z) \;\; s.t. \;\; x = f(y), y \in (-\infty, \infty) \;\; and \;\; z \in [0, b(f(y), y)]\}$$

where

(i) f is a continuous piecewise linear function of y such that $f(0) = x_0$ with $\max |\frac{\partial f}{\partial y}| < D$ (i.e. the angular deviation with respect to the direction of the axis $x = 0$ is lower than $\arctan(D)$);

(ii) b is a non-negative, bounded, continuous function of the two variables (x, y).

The crack pattern visible at the surface is $(f(y), y, 0)$ (see Figure 2).

The corresponding physical crack (or fracture) C_ϵ is an open neighborhood of σ. We suppose here that the set $C_\epsilon \cap \{y = y_0\}$ is approximatively the rectangle $(f(y_0) - \epsilon, f(y_0) + \epsilon) \times (0, b(f(y_0)))$.

Though a real fracture has hardly a rectangular section, this is an "order zero" approximation that simplifies the limit procedure from real to ideal crack and, especially, makes simpler the construction of a tool for the recognition of deep fractures. This tool gives good results also in the evaluation of fractures that deviate from the normal direction as shown in numerical simulations.

Finally, we define the domains

$$\Omega_0 = \Omega \setminus \sigma \tag{1}$$

and

$$\Omega_\epsilon = \Omega \setminus C_\epsilon. \tag{2}$$

3. Laser spot on the top surface of an intact slab. The background temperature

In Laser Spot Thermography, a specimen (in our case a concrete slab initially at the environment temperature U^0) is heated by means of a laser device. For the reasons explained in Section 2 the slab can be represented by the half-space $\Omega = \{z \geq 0\}$. When the specimen is not corroded or cracked, its temperature increase $u = T - U^0$ fulfills the heat conduction equation (T is the absolute temperature)

$$\rho c u_t(x, y, z, t) = \kappa \Delta u(x, y, z, t) \tag{3}$$

with $(x, y, z) \in \Omega$ and $t \in (0, t_{\max}]$ provided that the following boundary conditions are satisfied

$$-\kappa u_z(x, y, 0, t) + Hu(x, y, 0, t) = \phi(x, y)\chi_{(0,t_L)}(t) \tag{4}$$

$$lim_{x^2+y^2+z^2\to\infty} u^2 = 0. \tag{5}$$

Here, $\chi_E(x) = 1$ if $x \in E$ and $\chi_E(x) = 0$ elsewhere. The physical parameters ρ, c and κ in (3) are density, specific heat and thermal conductivity of the material under investigation. The laser spot is assumed to have a Gaussian shape

$$\phi(x, y) = \phi_L e^{-\frac{x^2+y^2}{\delta_L^2}} \tag{6}$$

Laser is ON from $t = 0$ to $t = t_L < t_{\max}$. H is the heat transfer coefficient at the heated surface $z = 0$, the constant $\phi_L > 0$ is the maximum power per unit surface of the laser source, while the "standard deviation" parameter $\delta_L > 0$ measures the spread of the Laser Spot.

As we are dealing with "relative" temperatures, the initial u value is:

$$u(x, y, z, 0) = 0 \tag{7}$$

in Ω.

The solution of the above IBVP for an undamaged specimen is called "background temperature". It is denoted by u_0 and it can be obtained in terms of the Green's function for the half-space space with a Robin boundary condition (also called instantaneous point-source solution [21]) at the surface $z = 0$, representing the temperature response to a Dirac's delta in time and space:

$$\begin{aligned} G_{ips}(x, y, z, t|x', y', z', \tau) &= \frac{e^{\frac{-(x-x')^2-(y-y')^2}{4\alpha(t-\tau)}}}{8[\pi\alpha(t-\tau)]^{\frac{3}{2}}}\left[e^{\frac{-(z-z')^2}{4\alpha(t-\tau)}} + e^{\frac{-(z+z')^2}{4\alpha(t-\tau)}}\right] \\ &\quad - \frac{he^{h(z+z')+\alpha h^2(t-\tau)-\frac{(x-x')^2+(y-y')^2}{4\alpha(t-\tau)}}}{4\pi\alpha(t-\tau)\mathrm{erfc}\left(\frac{z+z'}{2\sqrt{\alpha(t-\tau)}} + h\sqrt{\alpha(t-\tau)}\right)} \end{aligned} \tag{8}$$

where $h = \frac{H}{\kappa}$, and α is the diffusivity of the material. The second term in the right hand side of (8) represents a correction to the "standard" instantaneous point source solution of the heat equation, needed to fulfill the heat condition at $z = 0$.

To obtain the temperature in a point at time t the instantaneous point source (8) must be integrated in exchange $d\tau$ between 0 and t, obtaining the Green's function for a continuous point source located on the $z' = 0$ plane.

$$G_{cps}(x, y, z, t|x', y', 0) = \frac{\mathrm{erfc}\left(\frac{r}{2\sqrt{\alpha t}}\right)}{2\pi\alpha r} - g_{corr}(x, y, z, t|x', y', 0) \tag{9}$$

where $\mathrm{r}^2 = (\mathrm{x} - \mathrm{x}')^2 + (\mathrm{y} - \mathrm{y}')^2 + \mathrm{z}^2$. Note that in the following, the notation $(x, y, z, t|x', y', z', \tau)$ means: "effect in (x, y, z) at time t of a source in (x', y', z') at time τ".

For ordinary values of the heat transfer coefficient H it is easy to show that, for any finite $r = \sqrt{(x - x')^2 + y'^2}$, and for any time t, the following relationship holds:

$$g_{corr}(r, t) = \frac{h}{2\pi\alpha}\int_0^t \frac{\mathrm{erfc}(h\sqrt{\alpha(t-\tau)})}{t-\tau} e^{(\alpha)h^2(t-\tau)}e^{-r^2/[4\alpha(t-\tau)]}d\tau \ll \frac{\mathrm{erfc}(r/(2\sqrt{\alpha t}))}{2\pi\alpha r}. \tag{10}$$

It means that the Green's function (9) for a source belonging to the $z' = 0$ plane can be simplified and the temperature $u(x, y, z, t)$ obtained by convolving

G_{cps} with the laser power function $\phi(x', y')$ located on the $z' = 0$ plane is

$$u_0(x, y, z, t) = \int_{-\infty}^{\infty} \int_{-\infty}^{\infty} \frac{\operatorname{erfc}\left(\frac{\sqrt{(x-x')^2+(y-y')^2+z^2}}{2\sqrt{\alpha t}}\right)}{2\pi\alpha\sqrt{(x-x')^2+(y-y')^2+z^2}} \frac{\phi(x', y')}{\rho c} dx' dy'. \quad (11)$$

A crack is essentially a 2D structure, because its largest dimension (taken as y-directed) on the surface is usually several times greater than the smallest one (x-directed). In such case, the physical situation can be represented by means of a 2D model and the Greens' functions accordingly change from instantaneous/continuous point sources to instantaneous/continuous line source.

The laser illumination is simulated by a line source, infinitely extending in the y direction, as assumed for the crack, therefore it consists in a Gaussian function depending on x only:

$$\phi(x) = \phi_L e^{-\frac{x^2}{\delta_L^2}} \quad (12)$$

The Green's function for a continuous line source is obtained from (8) by integrating it in dy' between $-\infty$ and ∞ (to obtain an instantaneous line source) and successively integrating in $d\tau$ between 0 and t. As we are interested in the solution on the axis $z = 0$, the Green's function is:

$$G_{cls}(x, 0, t|x', z') = -\frac{\operatorname{Ei}(-\frac{r^2}{4\alpha t})}{2\pi\alpha} - \int_0^t \frac{h e^{hz' + \alpha h^2 (t-\tau) - \frac{(x-x')^2}{4\alpha(t-\tau)}} d\tau}{2\sqrt{\pi\alpha(t-\tau)} \operatorname{erfc}\left(\frac{h}{2\sqrt{\alpha(t-\tau)} + h\sqrt{\alpha(t-\tau)}}\right)} \quad (13)$$

where Ei is the exponential integral function, and $r^2 = (x - x')^2 + z'^2$.

The temperature $u_0(x, t)$ is eventually obtained by convolving the Green's function (13) with the laser power function $\phi(x')$ which is located on the $z' = 0$ axis:

$$u_0(x, t) = \int_{-\infty}^{\infty} G_{cls}(x, 0, t|x', 0) \frac{\phi(x')}{\rho c} dx'. \quad (14)$$

The integral term in the right hand side of (13) can usually be neglected for the same reasons expressed in the 3D case.

4. The direct model: heat conduction in a cracked specimen

Recovering the perturbation C_ϵ of the domain Ω from thermal data collected over its accessible side, requires the solution of a non linear inverse problem for the heat equation. Here, we study some aspects of the underlying direct model. In order to ligthten the notation we set the problem in 2D so that the undamaged domain is $\Omega = (-\infty, \infty) \times (0, \infty)$ while the physical crack is the rectangle

$$C_\epsilon = \{(x, z) \;\; s.t. \;\; x \in (x_0 - \epsilon, x_0 + \epsilon) \;\; and \;\; b > z > 0\}. \quad (15)$$

Although actually the crack has a time evolution, it can be considered stationary on the time scale of the experiment.

4.1. Ideal cracks as limit of physical cracks

First, we observe that the thermal conductivity inside a fracture is always a positive number, possibly a very small one as in the case of air filled defects. Hence, any physical crack C_ϵ is supposed to have a non-zero conductivity coefficient κ_c. When the heat conduction through the fracture is negligible, we say that the crack is insulating and set $\kappa_c = 0$.

In order to study conducting and insulating fractures, we consider the system of two parabolic equations

$$\rho c u_t(x, z, t) = \kappa \Delta u(x, z, t) \tag{16}$$

with $(x, z) \in \Omega_\epsilon = \Omega \setminus C_\epsilon$ and $t \in (0, t_{\max}]$ and

$$\rho_c c_c u_t(x, z, t) = \kappa_c \Delta u(x, z, t) \tag{17}$$

with $(x, z) \in C_\epsilon$ and $t \in (0, t_{\max}]$ (the subscript c means "crack").

The boundary condition for $z = 0$ is

$$-\kappa u_z(x, 0, t) + H u(x, 0, t) = \phi_L e^{-\frac{x^2}{\delta_L^2}} \chi_{(0,t_L)}(t) \tag{18}$$

for $x \notin (x_0 - \epsilon, x_0 + \epsilon)$ and $t < t_L < t_{max}$,

$$-\kappa u_z(x, 0, t) = 0. \tag{19}$$

for $x \in (x_0 - \epsilon, x_0 + \epsilon)$ and $t < t_L < t_{\max}$

The temperature increase u (introduced at the beginning of section 3) vanishes at infinity and the initial temperature is

$$u(x, z, 0) = 0 \tag{20}$$

in Ω.

Let u^ϵ and u_c^ϵ fulfill the IBVP, respectively in Ω_ϵ and C_ϵ, for all times t. At the air-concrete interface $\{x = x_0 \pm \epsilon,\ z \in (0, b)\}$ we have transmission conditions for temperature

$$u^\epsilon(x, z, t) = u_c^\epsilon(x, z, t)$$

and heat flux

$$\kappa u_x^\epsilon(x, z, t) = \kappa_c u_{cx}^\epsilon(x, z, t) \tag{21}$$

where the subscript x means partial derivative of u^ϵ and u_c^ϵ.

In the limit for $\epsilon \to 0$ we have that $u^\epsilon \to u_\sigma$ where u_σ fulfills the heat equation in $\Omega_\sigma \times (0, t_{max}]$ and the same boundary conditions of u^ϵ. Furthermore, the transmission conditions (21) become Robin boundary conditions on the two sides of the crack :

$$\kappa u_{\sigma x}(x_0, z, t) + H_{eff}(u_\sigma(x_0^-, z, t) - u_0(x_0, z, t)) = 0 \tag{22}$$

$$-\kappa u_{\sigma x}(x_0, z, t) + H_{eff}(u_\sigma(x_0^+, z, t) - u_0(x_0, z, t)) = 0 \tag{23}$$

where $H_{eff} = \lim_{\epsilon \to 0} \frac{\kappa_c}{2\epsilon}$. The Robin conditions on the crack come from the analogy with vanishing coatings [22] thanks to the relation

$$u_0(x_0, z, t) = \frac{u_\sigma(x_0^-, z, t) + u_\sigma(x_0^+, z, t)}{2} \tag{24}$$

corollary of the Humps Theorem in [17].

Theorem. We have for all σ

$$u_\sigma(x_0 + \xi, z, t) + u_\sigma(x_0 - \xi, z, t) = u_0(x_0 + \xi, z, t) + u_0(x_0 - \xi, z, t) \tag{25}$$

where $t \in (0, t_{\max}]$, $\xi \in (-\infty, \infty)$ and $x_0 > 0$.

Robin conditions are in agreement with the definition of *heat transfer coefficient* (see for example [21] section 1.9).

The evaluation of H_{eff} is a problem in itself when the fracture is actually an interface between different materials [23]. H_{eff} is referred to also as the inverse of the thermal resistance of the interface.

We have the following three cases :

1. Insulating crack if $H_{eff} = 0$;
2. Conducting crack if $\infty > H_{eff} > 0$
3. Perfectly conducting crack if $H_{eff} = \infty$.

Suppose that we are using the ideal crack σ in order to model a real fracture of width w_c and internal conductivity κ_c. In this case, we have $H_{eff} \approx \frac{\kappa_c}{w_c}$.

Remark 1. The case of perfectly conducting crack is out of the limits of the present paper. In that case, no temperature gap is observed (for all values of t) between the opposite sides of the crack. It includes, for example, the case in which $\kappa_c = \kappa$ i.e. there is no fracture if also density and specific heat coincide. In the limit case of perfect conducting crack with $\kappa_c = \infty$ the temperature is constant on the whole crack (see for example [24]).

Remark 2. In case we cannot neglect its dependence of the fracture width, H_{eff} is inversely proportional to w as a first approximation.

4.2. Heuristic representation of the surface temperature of the damaged specimen

The Humps Theorem suggests to expand the temperature of the accessible boundary $z = 0$ in terms of the background temperature and some particular weight functions in a generalization of the one-dimensional solution obtained in [25] by means of the method of images.

We assume along this section that the laser spot heats only one side of the crack (in particular for $x < x_0$). Hence, in presence of an insulating, ideal crack we have (for $\xi \geq 0$, $z \geq 0$ and $t \in (0, t_{max}]$)

$$u_\sigma(x_0 - \xi, z, t) = u_0(x_0 - \xi, z, t) + u_0(x_0 + \xi, z, t) \tag{26}$$

and

$$u_\sigma(x_0 + \xi, 0, t) = 0. \tag{27}$$

More generally, the surface temperature of the slab, in presence of the conducting crack σ of length b, can be written for all $t \in (0, t_{max})$ in terms of the background temperature u_0, a weight $\beta_1(\xi, t; H_{eff}) \geq 0$ (related to width and conductivity of the real crack) and a positive function $E_b(\xi, t)$. The term E_b accounts for heat passing over (when the laser is ON), under and (in the extension to 3D models) around the fracture.

We have

$$u_\sigma(x_0 - \xi, 0, t) \approx u_0(x_0 - \xi, 0, t) + \beta_1 u_0(x_0 + \xi, 0, t) - E_b(\xi, t) \tag{28}$$

and

$$u_\sigma(x_0 + \xi, 0, t) \approx (1 - \beta_1) u_0(x_0 + \xi, 0, t) + E_b(\xi, t). \tag{29}$$

In case of insulating crack it is $\beta_1 = 1$. In this case, some properties of E_b come to light from numerical simulations:

(i) The function E_b vanishes when the depth b is large enough while

$$\lim_{b \to 0} E_b(\xi, t) = E_0(\xi, t) = u_0(x_0 + \xi, 0, t)$$

(ii) The function E_0 is continuous everywhere but not right-hand differentiable for $\xi = 0$. Since $\forall b > 0$ it is $\frac{\partial E_b}{\partial x}(0, t) = 0$ we have $\lim_{b \to 0} \frac{\partial E_b}{\partial x}(0, t) = 0$. It means that $u_\sigma^b \to u_0$ for $b \to 0$ but $lim_{b \to 0} u_{\sigma x}^b(x_0, 0, t) = 0 \neq u_{0x}(x_0, 0, t)$.

When we deal with a conducting crack, the quantity of heat that passes through the fracture is proportional to H_{eff} and b. We already observed that E_b can be neglected if b is large enough. Furthermore, there is a range of b in which E_b can be linearized, obtaining

$$E_b(\xi, t) \approx \beta_0(b; \xi, t) u_0(x_0 - \xi).$$

Hence, if we set $\beta(H_{eff}, b; \xi, t) = \beta_1(H_{eff}; \xi, t) - \beta_0(b; \xi, t)$, it is

$$u_\sigma(x_0 - \xi, 0, t) \approx u_0(x_0 - \xi, 0, t) + \beta u_0(x_0 + \xi, 0, t) \tag{30}$$

and

$$u_\sigma(x_0+\xi,0,t) \approx (1-\beta)u_0(x_0+\xi,0,t). \tag{31}$$

This formula fits very well numerical simulations in the range of b in which we are able to determine the depth of the fracture (see section 6.2). A rigorous mathematical analysis of E_b, beyond the limits of the present work, is in [17].

5. Evaluation of the depth of a visible fracture by means of a Laser Spot generated for a finite time interval.

Suppose that we are able to reveal the presence of a fracture by means of images in the visible range of frequencies or by means of a passive infrared scanning of the surface of the specimen. A first rough analysis should be done pointing the laser spot over the fracture. In this way, the thermal map after a suitable time interval would give hints about the symmetry of the fracture at least in an external layer of the slab. In what follows we assume that no asymmetries are revealed and the width of the fracture is constant with respect to the depth. The effects of possible deviations from the orthogonal direction will be discussed in the section about numerical simulations.

In order to evaluate the depth of a fracture orthogonal with respect to the surface, we apply a laser spot on a point P_L close to the crack, for a time interval $(0, t_L]$. In the meanwhile (and for an additional time after laser is OFF) we collect a sequence of temperature maps of the surface by means of an infrared camera. We observe a gap in the temperature on opposite sides of the fracture. Our goal is to determine a relation between this gap and the depth of the fracture. A similar task is carried out in [26] using the so-called ghost point model to reconstruct microfractures in steel manufacts.

Though our problem looks like a typical one in inverse heat conduction we know that a thin deep defect like C_ϵ cannot be detected, in practice, from the knowledge of thermal contrast by means of the usual methods in active pulsed thermography [27]. In fact, Laser Spot Thermography is a local technique that depends strongly on the distance between the application point P_L and the crack. Our chances to evaluate the depth of the fracture come from the choice of P_L as close as possible to the crack while almost all the power of the laser spot is given on one side only. Starting from the approximated representation (30)-(31), in this section we derive an heuristic relation between available temperature data and the unknown depth of the fracture.

The surface temperature on the opposite sides of an ideal crack shows a gap (u_ϵ is defined in section 4.1)

$$g(b, H_{eff}, t) = u_\epsilon(x_0-\epsilon,0,t) - u_\epsilon(x_0+\epsilon,0,t) \tag{32}$$

which depends on the depth b, on the heat transfer coefficient $H_{eff} \approx \frac{\kappa_c}{2\epsilon}$ through the crack (see section 4.1) and on the choice of the instant $t \in (0, t_{max}]$.

Let $v_0(x, z, t)$ and $w_0(x, z, t)$ be the temperatures of the half-space $z \geq 0$ determined by the laser spots $\phi_L e^{-\frac{x^2}{\delta_L^2}} \chi_{(-\infty, x_0-\epsilon)}(x)$ and $\phi_L e^{-\frac{x^2}{\delta_L^2}} \chi_{(x_0+\epsilon,\infty)}(x)$ respectively. It is remarkable that the sum $v_0 + w_0$ (effective background temperature) could be quite different from the actual background temperature u_0 studied in section 3 (for example, see Figure 3).

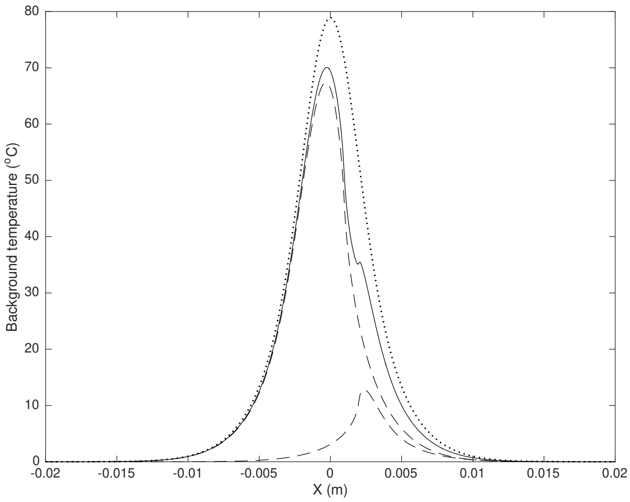

Figure 3: Comparison among u_0 (dotted line), v_0 and w_0 (dashed lines) and $v_0 + w_0$ (solild line)

We adapt the heuristic representation (30)-(31) of the surface temperature to the assumption of a positive not negligible ϵ. The external temperature of the damaged slab is now $u_\epsilon = v_\epsilon + w_\epsilon$ instead of u_σ. When the crack is insulating and sufficiently deep, we have

$$v_\epsilon(x_0 - \xi, 0, t) = v_0(x_0 - \xi, 0, t) + v_0(x_0 + \xi, 0, t) \tag{33}$$

$$w_\epsilon(x_0 - \xi, 0, t) = 0 \tag{34}$$

and

$$v_\epsilon(x_0 + \xi, 0, t) = 0 \tag{35}$$

$$w_\epsilon(x_0 + \xi, 0, t) = w_0(x_0 + \xi, 0, t) + w_0(x_0 - \xi, 0, t). \tag{36}$$

As for conducting fractures, we have

$$v_\epsilon(x_0 - \epsilon - \xi, 0, t) = v_0(x_0 - \epsilon - \xi, 0, t) + \beta_\epsilon v_0(x_0 - \epsilon + \xi, 0, t) \tag{37}$$

$$w_\epsilon(x_0 - \epsilon - \xi, 0, t) = (1 - \beta_\epsilon) w_0(x_0 - \epsilon - \xi, 0, t) \tag{38}$$

and

$$v_\epsilon(x_0 + \epsilon + \xi, 0, t) = (1 - \beta_\epsilon) v_0(x_0 + \epsilon + \xi, 0, t) \tag{39}$$

$$w_\epsilon(x_0 + \xi, 0, t) = w_0(x_0 + \epsilon + \xi, 0, t) + \beta_\epsilon w_0(x_0 + \epsilon - \xi, 0, t). \tag{40}$$

The temperature gap between the opposite sides of the fracture becomes

$$\begin{aligned} u_\epsilon^- - u_\epsilon^+ \quad = \quad & v_0(x_0 - \epsilon) - v_0(x_0 + \epsilon) + w_0(x_0 - \epsilon) - w_0(x_0 + \epsilon) + \\ & \beta_\epsilon (v_0(x_0 - \epsilon) + v_0(x_0 + \epsilon) - w_0(x_0 - \epsilon) - w_0(x_0 + \epsilon)) \end{aligned} \tag{41}$$

Hence, we have

$$\beta_\epsilon(b) = \frac{u_\epsilon^- - u_\epsilon^+ - (v_0(x_0 - \epsilon) - v_0(x_0 + \epsilon) + w_0(x_0 - \epsilon) - w_0(x_0 + \epsilon))}{v_0(x_0 - \epsilon) + v_0(x_0 + \epsilon) - w_0(x_0 - \epsilon) - w_0(x_0 + \epsilon)} \equiv B. \tag{42}$$

It is easy to check that $\beta_\epsilon \to \frac{g(b, H_{eff}, t)}{2u_0(x_0, 0, t)}$ for $\epsilon \to 0$.

As for using formula (42), observe that the value of the r.h.s. B is determined from the knowledge of:

(i) the temperature gap $u_\epsilon^- - u_\epsilon^+$ (to be measured from the thermal maps) ;

(ii) the partial surface background temperatures v_0 and w_0 on both sides of the gap, computed by means of Green's function method.

Hence, the equality

$$\beta_\epsilon(b, H_{eff}, t) = B$$

can be regarded as an equation in the unknown b.

Observe that $\max_b \beta_\epsilon(b, H_{eff}, t)$ goes to zero for $t \to \infty$. When $\kappa_c = \kappa$ in C_ϵ (a special case of perfectly conducting crack) we have $\beta_\epsilon \equiv 0$ too (for all b and t).

The 2D finite element method (FEM) numerical simulations has been used to describe and analyze the temperature gap and the Green's function method to compute the background. As a result, we obtained a vector of N values of β_ϵ corresponding to N different depths of a rectangular crack in x_0 of width 2ϵ. Then, we derive the heuristic interpolation formula

$$\beta_\epsilon(b, H_{eff}, t) \approx \beta_1 - A_c(t) e^{-\frac{b - z_c(t))^2}{s_c(t)^2}}$$

where $A_c(t)e^{-\frac{z_c(t)^2}{s_c(t)^2}} = \beta_1$.

Finally,

$$b = z_c + s_c\sqrt{ln(\frac{A_c}{\beta_1 - B})}. \quad (43)$$

The above formula will be called β-*tool*.

It comes from the shape of $\beta_\epsilon(b, H_{eff}, t)$, as a function of b only, that its inversion allows to determine crack depth as long as $\frac{\partial\beta}{\partial b}$ is not too small. Observe that this limitation (depending on the value of t and on the diffusivity of materials at hand) is intrinsic and tightly connected to the ill-posedness of inverse problems for heat equation.

6. Modeling laser spot heating of a cracked concrete surface

In the previous section we have introduced the parameter β_ϵ corresponding to a real orthogonal crack whose width 2ϵ is given. We show now the results of a set of finite element simulations carried out by means of COMSOL Multiphysics® [28] in order to test some aspects of the β-tool defined at the end of Section 5.

6.1. Sensitivity analysis

β_ϵ is a function of the temperature gap between the opposite sides of the fracture (42), which depends on the crack depth b through the temperature gap g (the background temperature does not depend on b). In fact

$$\beta_\epsilon(b,t) = \frac{g(b,t) - F_1^\epsilon(v_0, w_0)}{F_2^\epsilon(v_0, w_0)} \quad (44)$$

with

$$F_1^\epsilon = v_0(x_0 - \epsilon) - v_0(x_0 + \epsilon) + w_0(x_0 - \epsilon) - w_0(x_0 + \epsilon)$$
$$F_2^\epsilon = v_0(x_0 - \epsilon) + v_0(x_0 + \epsilon) - w_0(x_0 - \epsilon) - w_0(x_0 + \epsilon)$$

The choice of time instant $tin(0, t_{max}]$, as discussed in Section 5, requires to study the sensitivity of $\beta\epsilon$ with respect to b.

The sensitivity analysis on β_ϵ is the study of the partial derivative $\partial\beta_\epsilon/\partial b$, and it coincides with the study of the time behavior of S(g, b) $= \partial g(b,t)/\partial b$.

The following figures refer to 2D simulations using the parameters summarized in Table 1

Figure 4 shows the normalized gap temperature, defined as the ratio between the gap g(b,t) and its limit value for large crack depths b: $g_{\text{NORM}} = g(b,t)/g(\infty,t)$ for different observation times: 20 s (circles), 40 s (+), 60 s (*), 80 s (x), 100 s (diamonds). It is clear that, in principle, the greater is the time

Table 1: Parameters of FEM simulations

	Crack dimension	
w	1	mm
b	from 1 to 18	mm
	FEM Parameters	
κ	1	W/(m K)
c	1000	J/(kg K)
ρ	1900	kg/m^3
H	0	W/(m^2 K)
ϕ_L	3.7×10^4	W/m^2
δ_L	2×10^{-3}	m
x_0	10^{-3}	m

the higher is the maximum detectable depth. But, of course, the greater is the time the lower is the temperature. The chosen observation time must be such to allow the gap value to be reliably detected by the thermocamera. It comes from figure 4 that times lower that t_L appear to be unsuitable because g_{NORM} reaches unity for very small values of b. Therefore, we look for a suitable value of t in the interval $(t_L, t_{max}]$.

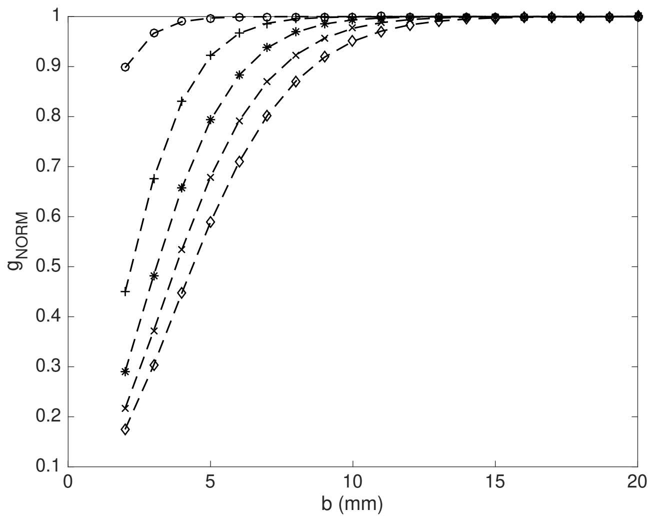

Figure 4: Normalized gap vs crack depth, at different times (see text)

The sensitivity S(g(b,t),b), shown in Figure 5, is a function of the crack depth b and, obviously, is very time dependent. The observation time, on the

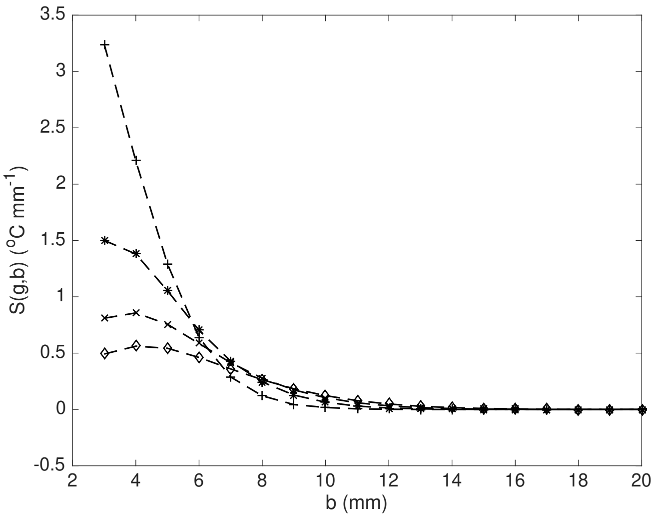

Figure 5: Sensitivity vs crack depth, at different times (see text)

base of the sensitivity analysis, should be chosen such to have a non-zero S value at the highest possible depth b.

6.2. Numerical experiments on simulated cracks

The crack is assumed to be orthogonal to the direction of the major principal stress (i.e. three-point bending beam), as reported in Figure 6, thus we consider the cracked concrete sample loaded under Mode I [5].

In the aim of characterizing the defect which affects the specimen, the laser spot is activated for 20 seconds. Then we observe the temperature decay for about one minute. The initial temperature U^0 has been set equal to 20^oC in the whole domain.

We consider at first the damaged concrete block $\Omega_\epsilon = \Omega \setminus C_\epsilon(b)$ where $C_\epsilon(b)$ is a linear normal crack with width $w = 2\epsilon = 1$ mm and depth b ranging from 1 mm to 18 mm. This finite set of rectangular cracks is used to build a vector of values of the parameter $\beta_\epsilon(b)$. The curve obtained interpolating these data like in section 5 gives us a pointwise correspondence between the parameter β_ϵ (that we can derive from available data corresponding to any unknown fracture) and the depth of a normal fracture. We have calculated the value of β_ϵ for the twelve assumed values in the range of the depth at the time $t = 80$ sec i.e. 60 sec after the shut off of the laser. The curve plotted in Figure 7 is the graph of $\beta_\epsilon(b) = \beta_1 - A\exp(-\frac{(b-z)^2}{s^2})$ for $b \in (0, 0.018)$ obtained by interpolation. It is clear, from the shape of the curve, that a depth greater than 10 mm can hardly be determined. Hence, our method (contactless and fast) can be used

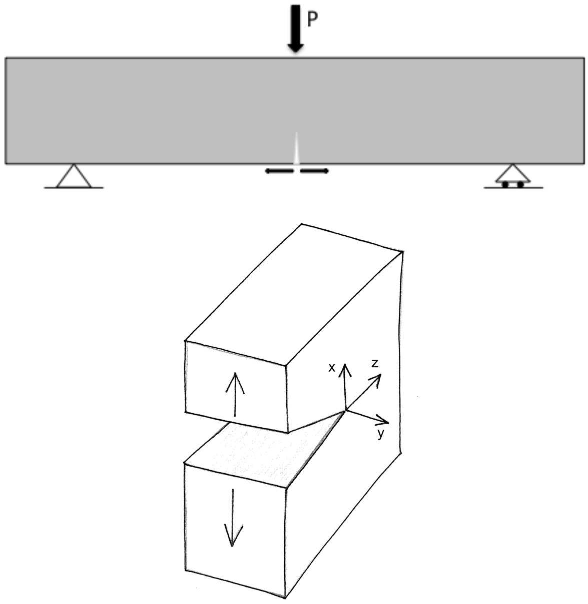

Figure 6: A single edge crack in a semi-infinite plate under uniform uniaxial stress (Mode I).

in practice to reveal which fractures are not superficial and require a further, possibly direct-contact, analysis.

To demonstrate the potentiality of the β-tool, this method has been tested on cracks with a more complex section. Five different cracks, denoted C_1 (sharp-ending rectangular crack), C_2 (rotated triangular section), C_3 (very irregular section), C_4 (shallow irregular section) and C_5 (deep sharp-ending rectangular crack) have been considered. They are presented in Figure 8. Beside each crack, the corresponding surface temperature for $t = 80$ sec is reported.

From the temperatures u_1, u_2, u_3, u_4 and u_5 plotted in Figure 8, and from the values of v_0 and w_0 computed with Green's function method (see section 3) we derived the values

$$\beta_{i\epsilon} = \frac{u_i^- - u_i^+ - (v_0(x_0-\epsilon) - v_0(x_0+\epsilon) + w_0(x_0-\epsilon) - w_0(x_0+\epsilon))}{v_0(x_0-\epsilon) + v_0(x_0+\epsilon) - w_0(x_0-\epsilon) - w_0(x_0+\epsilon)} \tag{45}$$

corresponding to C_i for $i = 1, 2, 3, 4, 5$. Then we derive the depth from the curve in Figure 7. The results are reported in the following Table 2.

The depth range reported in Table 2 for each crack, is substantially influenced by the shape and direction of the fracture. Clearly, regular and orthogonal cracks (i.e. C_1 and C_5) are better identified and our method gives back their

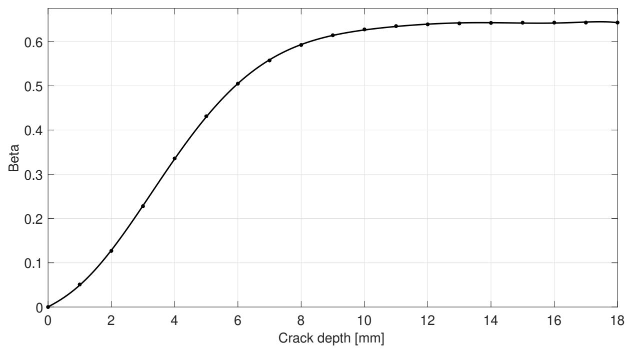

Figure 7: β-curve.

Table 2: Comparison between real crack and the β-tool results

Crack types	**Real depth [mm]**	**Beta value**	**Depth range [mm]**
Crack 1	10	0.6169	$9 \div 10$
Crack 2*	10	$0.5072 \div 0.6524$	$6 \div 18$
Crack 3	6	0.3115	$3 \div 4$
Crack 4	4	0.1632	$2 \div 3$
Crack 5	18	0.6430	≥ 17

depth very well. In those cases in which a complex and irregular shape is considered (i.e. C_2, C_3 and C_4) the prediction of the depth range is less careful, and so the use of this method requires that the operator shall implement more tests around the crack. Good evidence of this can be found looking at crack type C_2. Here, in particular, the laser spot has been applied on both edges of the fracture obtaining more accurate and reliable information about both the asymmetry and the depth of the damage. In the final analysis, therefore, it can be considered that the depth range of the crack corresponds to an average value of the tests (i.e. 12 mm as reported in Figure 9), which provide a good resolution for the real depth measurement.

One application of this approach is to distinguish cracks that could be dangerous for the structure from those that are not, by introducing a threshold above which further investigation is needed.

7. Application of the β-tool to experimental data

We show an application of the β-tool to data recorded in a LST experiment on a small fracture on a concrete beam. The external width of the crack varies between 2 and 3 mm and the crack depth, estimated by inserting a thin paper sheet, is of the order of 5-6 mm. The crack appears to shrink with depth.

The pulsed laser used in the experiment, working at wavelengths of 532 nm and 1064 nm and producing a beam with an average energy (mix of the two) of

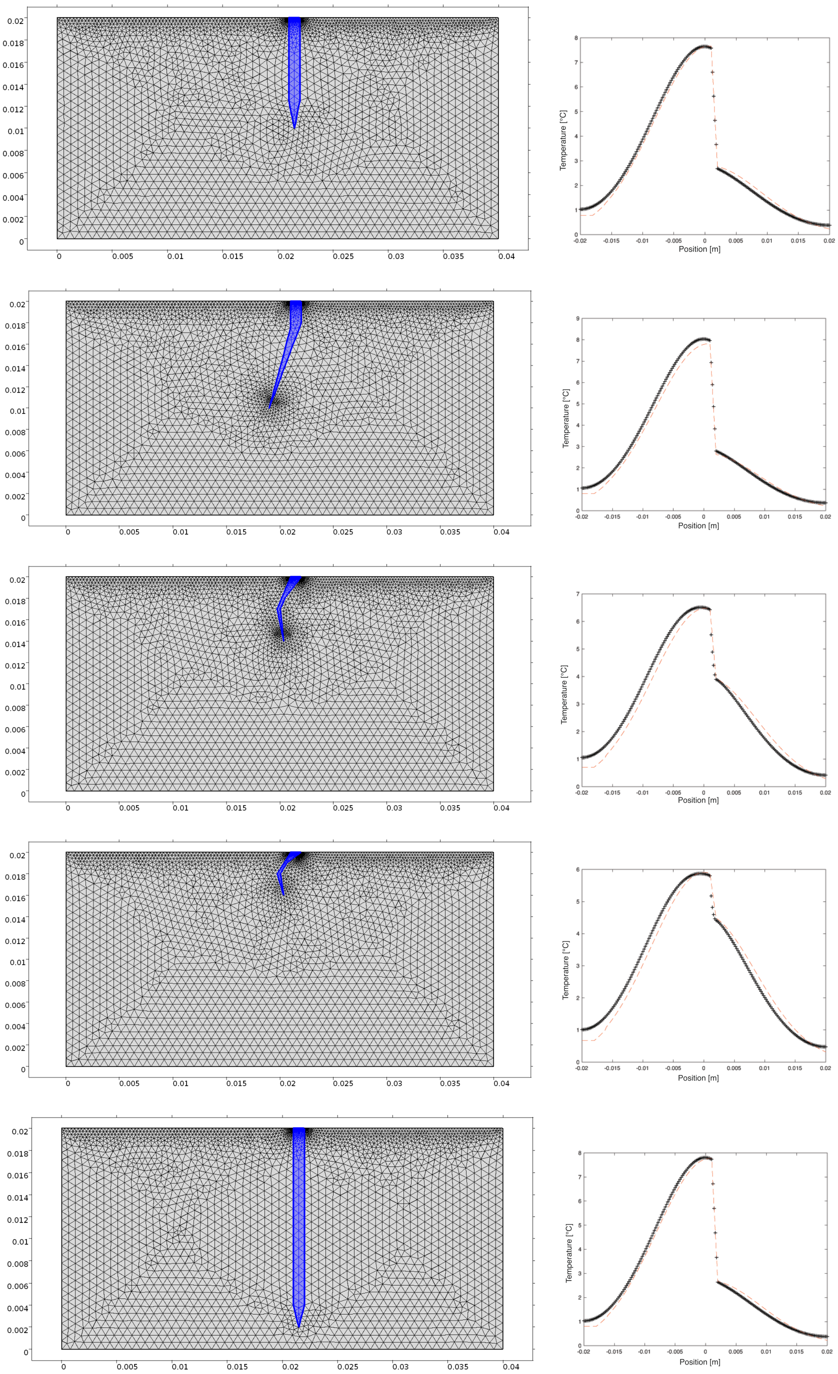

Figure 8: Different crack which are considered to validate the method.

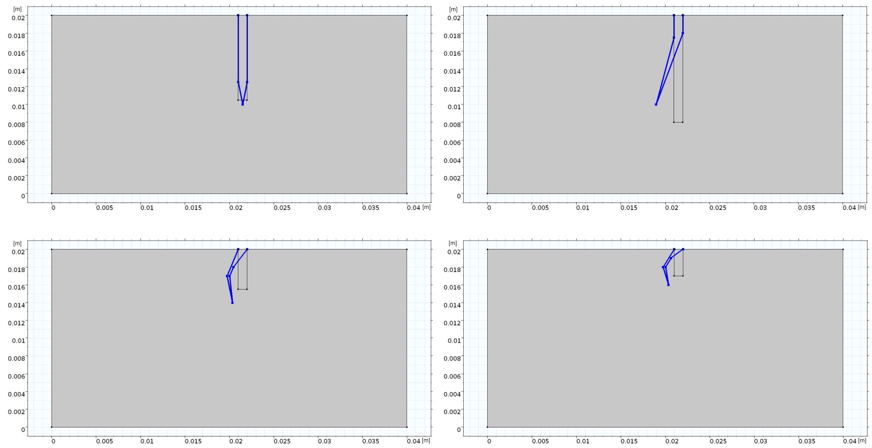

Figure 9: Real crack vs calculated depth range

about 40 mJ, produced a circular spot of about 2 mm diameter at a distance of 1 m from the wall. The emitted power was about 0.8 W, corresponding to a power density of the order of 1.6 W/cm^2. The center of the laser spot was 3.5 mm away from the crack edge.

7.1. 3D - 2D transformation of experimental data

Real thermographic data relate to the three-dimensional world, i.e. although the crack is essentially two-dimensional, the temperature behavior depends on the laser shape which is a spot, not a linear source as assumed in the simulations.

Nevertheless, instead of implementing a 3D numerical model, which is computationally heavy, we prefer to transform 3D experimental data into "equivalent" 2D data. As we will show in the following subsections, this is possible if we are interested in data belonging to the symmetry plane of the laser source, taken as the XZ plane of the 2D model.

7.1.1. 3D - 2D transformation for a homogeneous half-space

The continuous-source Green's functions for 3D (point-source) and 2D (line-source) half-spaces are respectively:

$$G_{3c} \sim \frac{\mathrm{erfc}(-\frac{r}{2\sqrt{\alpha t}})}{2\pi\alpha r} \tag{46}$$

$$G_{2c} \sim -\frac{\mathrm{Ei}(-\frac{\rho^2}{4\alpha t})}{2\pi\alpha} \tag{47}$$

where $\rho^2 = (x-x')^2 + z'^2$ and $r^2 = (x-x')^2 + (y-y')^2 + z'^2$.

Assuming a "rectangular" laser source of width 2ϵ on the plane (line, in the 2D case) $z = 0$, the temperatures $u_3(x, y, z, t)$ and $u_2(x, z, t)$ are obtained by convolving the Green's functions (46) and (47) with the laser power function $\phi(x', y')$ ($\phi(x')$ in the ”D case) which is located on the $z' = 0$. In particular, on the "accessible" surface $z = 0$:

$$u_3(x, y, t) = \frac{\phi_0}{\rho c} \int_{-\epsilon}^{\epsilon} \int_{-\epsilon}^{\epsilon} G_{3c}(x, y, 0, t|x', y', 0) dx' dy' \tag{48}$$

$$u_2(x, t) = \frac{\phi_0}{\rho c} \int_{-\epsilon}^{\epsilon} G_{2c}(x, 0, t|x', 0) dx' \tag{49}$$

ρ and c being the density and specific heat of the material, and ϕ_0 the intensity of the heat flux. The assumption of a rectangular source instead of a gaussian one simplifies the computation, and it negligibly affects the results because the temperature produced by such a source shape is anyway gaussian after a small time interval.

The notation in (46) and (47) is a short-cut, meaning that the Green's functions for the heating phase ($t \leq t_L$) and for the decay phase ($t > t_L$) are given by the following expressions:

$$G_{3c}(x, y, z, t|x', y', 0) = \begin{cases} \frac{1}{2\pi\alpha r} \mathrm{erfc}(-\frac{r}{2\sqrt{\alpha t}}) & t \leq t_L \\ \frac{1}{2\pi\alpha r} \left[\mathrm{erfc}(-\frac{r}{2\sqrt{\alpha t}}) - \mathrm{erfc}(-\frac{r}{2\sqrt{\alpha(t-t_L)}}) \right] & t > t_L \end{cases} \tag{50}$$

$$G_{2c}(x, z, t|x', 0) = \begin{cases} -\frac{1}{2\pi\alpha r} \mathrm{Ei}(-\frac{\rho^2}{4\alpha t}) & t \leq t_L \\ -\frac{1}{2\pi\alpha r} \left[\mathrm{Ei}(-\frac{\rho^2}{4\alpha t}) - \mathrm{Ei}(-\frac{\rho^2}{4\alpha(t-t_L)}) \right] & t > t_L \end{cases} \tag{51}$$

Comparing (48) with (49) it is clear that, given the temperature $U_3(x, 0, 0, t)$ **measured** on the x axis at time t, we can formally obtain a 2D-equivalent temperature $U_2(x, t)$ by:

$$U_2(x, 0, t) = U_3(x, 0, 0, t) \frac{\int_{-\epsilon}^{\epsilon} G_{2c} dx'}{\int_{-\epsilon}^{\epsilon} \int_{-\epsilon}^{\epsilon} G_{3c} dx' dy'} \tag{52}$$

7.1.2. 3D - 2D transformation for a cracked half-space

Assuming the approximate correctness of the β model for the cracked 2D-region, on the x axis (x_0 being the crack abscissa):

$$u_{\sigma 2}(x, 0, t) = \begin{cases} u_0(x, t) + \beta u_0(2x_0 - x, t) & x < x_0 \\ (1 - \beta) u_0(x, 0, t) & x > x_0 \end{cases} \tag{53}$$

the temperature $u_{\sigma 2}$ can be expressed in terms of the background Green's function, when β is known.

The same is true in the 3D case, therefore it appears reasonable (and it is numerically demonstrated) that a relationship like (52) holds as well:

$$U_{\sigma 2}(x, 0, t) \approx U_{\sigma 3}(x, 0, 0, t) \frac{\int_{-\epsilon}^{\epsilon} G_{2c} dx'}{\int_{-\epsilon}^{\epsilon} \int_{-\epsilon}^{\epsilon} G_{3c} dx' dy'} \tag{54}$$

because the β value, quantifying the amount of heat passing through the crack, can be reasonably assumed the same in the 2D and 3D case at least on the x axis, i.e. on the symmetry plane $y = 0$ of the 3D model.

Figure 10 compares the temperature on the x axis at time $t = 40s$ in the decay phase, i.e. for $t_L = 20s$, numerically computed in the 2D case (red solid line) and obtained by the 3D-2D transformation (54) (black dashed line).

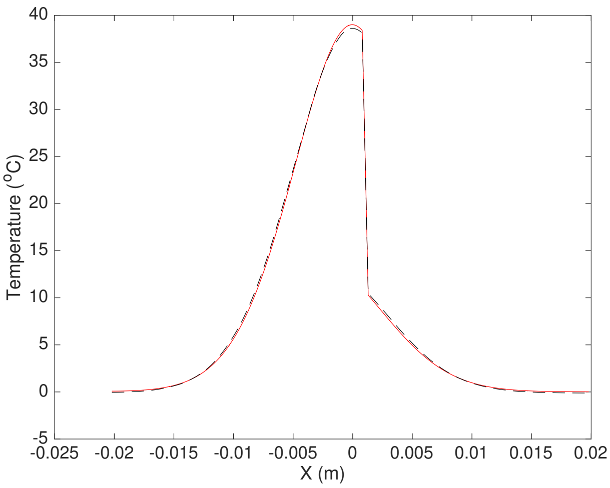

Figure 10: Temperature 20 s after laser OFF, in the 2D case (red, solid) and in the 3D case transformed to 2D (black, dashed)

7.2. Experimental determination of the crack depth

Figure 11 shows the temperature at time t = 40 s (i.e. 20 s after laser OFF) on the symmetry axis X of the thermal distribution taken from the thermographic image. The temperature values actually are temperature differences with respect to the initial value.

The transformation to a 2D distribution, together with the computed background temperature, is shown in Figure 12.

The presence of heat diffusion paths not taken into account by the model is evident in the temperature behavior immediately at the right of the crack. While the left edge of the temperature gap is easy recognizable (point P_1), to objectively (and automatically) obtain the right edge P_2 we proceed as follows.

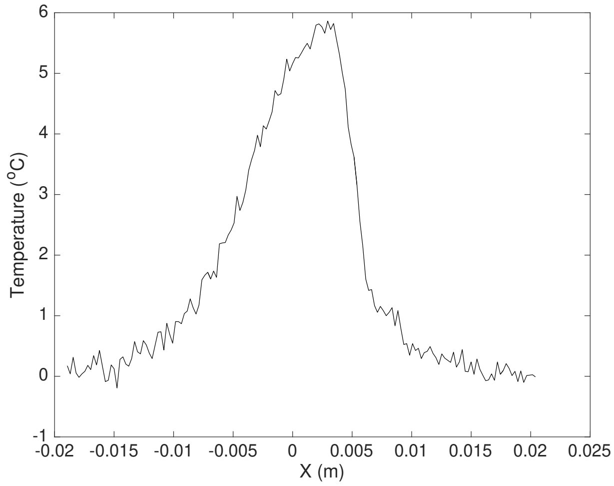

Figure 11: Temperature on the X axis, 20 s after laser OFF

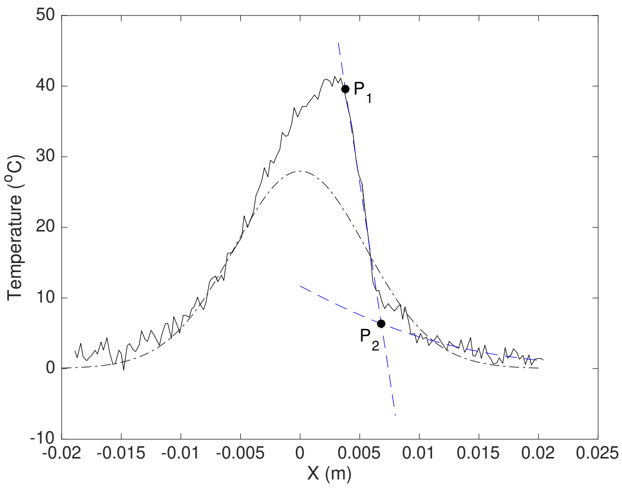

Figure 12: 2D Temperature on the X axis, 20 s after laser OFF (solid line). Background temperature (dash-dot line).

We know that the temperature behavior immediately at the right of the crack edge should be a gaussian, and that the temperature drops off linearly across the crack. Therefore, the procedure consists in fitting a gaussian on the data immediately at the right of the temperature "anomaly" (discrepancy among model and experiment), and perform a linear fitting on the data across the crack opening, as shown in Figure 12. The crossing P_2 among those fitting curves identifies the right edge of the gap. Eventually, we are able to compute the β value (45) in terms of the temperatures in P_1 and P_2, respectively u_1 and u_2, and of the background temperatures v_1^0 and v_2^0 at the same points:

$$\beta = \frac{u_1 - u_2 - (v_1^0 - v_2^0)}{v_1^0 + v_2^0} = 0.71 \tag{55}$$

where the w background terms have been dropped because the source is totally at the left of the crack opening.

The above β value is used as an input into the β-tool curve, shown in figure 13, computed for the experimental parameters (power density, average crack width, distance of laser spot from crack edge).

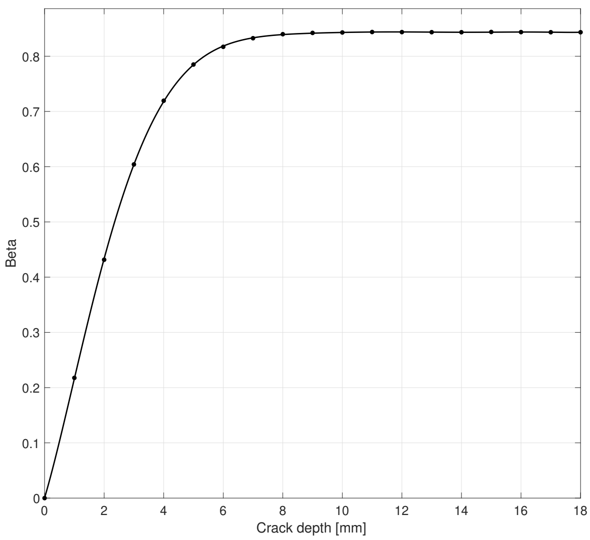

Figure 13: β-tool curve for the experiment

The crack depth obtained from the curve is about 4 mm, slightly underestimated with respect to the actual depth, as expected because of the crack shrinking.

Conclusions

We have developed a computational procedure for evaluating the crack depth on a concrete slab specimen by means of Laser Sport Thermography. The knowledge of the thermal gap between the two sides of the fracture allows estimating the crack depth by expressing the surface temperature of the damaged slab in terms of its background temperature.

The optimal observation time, evaluated by means of a sensitivity analysis, is about 60 seconds after the switch off of the laser.

The gap is derived from thermal maps of the surface (here we used COMSOL simulations of data collection) while the temperature of the undamaged specimen (background temperature) have been calculated by means of Green's function method.

By means of systematic simulations we established a one-to-one relation between the adimensional parameter β_ϵ (normalized thermal gap) and the depth b of a vector of model fractures orthogonal to the accessible surface. The interpolating curve $(b, \beta_\epsilon(b))$ has been used like a ruler (β-tool) to evaluate the depth of unknown fractures of various geometry. The expression

$$\beta_\epsilon(b) \approx \beta_1 - Ae^{-\frac{(b-z)^2}{s^2}}$$

is derived heuristically.

Though the β-tool accounts for straight vertical fractures with constant width only, it give also an "order zero" approximation of the depth of curved fractures of variable width. The evaluation of an effective depth for such fractures can be improved by means of a symmetry analysis based on the symmetrical heating of both sides of the fracture.

The β-tool has been tested on simulations (see figure 9) and on experimental data as described in section 7. In both cases, in our opinion, the evaluation of the fracture is quite good.

Finally, depth is evaluated for cracks shorter than 15mm. Deeper fractures are addressed to more accurate direct-contact analysis (for example dye penetrant inspection).

Acknowledgment

This work has been supported by the FAR-FIS research project "TOSCA-FI" funded by Tuscany Region.

References

[1] R.J. Woodward, Non destructive testing methods for concrete bridges, Research Report 250 Transport and road research lab, Crowthorne, Berkshire UK (1989)

[2] https://www.giatecscientific.com/education/cracking-in-concrete-procedures/ (2014)

[3] https://framcos.org/FraMCoS-9/Book-Abstracts/Book-Abstracts-9.pdf (2016)

[4] C. Andrade, C. Alonso and F.J. Molina, Cover cracking as a function of rebar corrosion: Part I - Experimental test, Material and Structures, 26, 453-464 (1993)

[5] Z. P. Bazant, Concrete fracture models: testing and practice. Engineering fracture mechanics 69, 165-205 (2002)

[6] A. Michel, M. R. Geiker, H. Stang , J. F. Olesen A. O. S.and Solgaard , Modeling formation of cracks in concrete cover due to reinforcement corrosion, Fracture Mechanics of Concrete and Concrete Structures - Assessment, Durability, Monitoring and Retrofitting of Concrete Structures- B. H. Oh, et al. (eds) 2010 Korea Concrete Institute, Seoul, ISBN 978-89-5708-181-5

[7] Y.Zhao and W. Jin (editors), Steel Corrosion-Induced Concrete Cracking Elsevier Cambridge MA USA 2016

[8] H. Wiggenhauser, C. Kopp, J. Timofeev and H. Azari, Controlled Creating of Cracks in Concrete for Non-destructive Testing. J Nondestruct Eval 37(67) (2018)

[9] T. Rabczuk, G. Zi, S. Bordas, H. Nguyen-Xuan, A geometrically non-linear three-dimensional cohesive crack method for reinforced concrete structures, Engineering Fracture Mechanics, 75, 4740-4758 (2008)

[10] T. Rabczuk, T.Belytschko, A three-dimensional large deformation meshfree method for arbitrary evolving cracks, Computer methods in applied mechanics and engineering, 196, 2777-2799 (2007)

[11] T. Rabczuk, T.Belytschko, Cracking particles: a simplified meshfree method for arbitrary evolving cracks, international Journal for Numerical Method in Engineering, 61:2316-2343 (2004)

[12] K.M. Hamdia, M.A. Msekh, M. Silani, T.Q. Thai, P.R. Budarapu, T. Rabczuk, Assessment of computational fracture models using Bayesian method, Engineering Fracture Mechanics, 205, 387-398 (2019)

[13] F.C. Sham, N. Chen and L. Long, Surface crack detection by flash thermography on concrete surface Insight (British Institute for Non-Destructive Testing), 50(5), 240-243 (2008)

[14] Y. Liang, H. Jialou and F. Choy, Quantitative NDE technique for assessing damages in beam structures, Journal of Engineering Mechanics 118(7), 1332-1345 (1990)

[15] R. Ruotolo and C. Surace, Damage assessment of multiple cracked beams: numerical results and experimental valida- tion, J. Sound Vibration 206(4), 567-588 (1997)

[16] X.P.V. Maldague. Theory and Practice of Infrared Technology for Nondestructive Testing, John Wiley and Sons, New York (2001)

[17] G. Inglese, R. Olmi and A. Scalbi, Characterization of a vertical crack by means of local thermal analysis. arXiv:1905.10166 (2019)

[18] J.C. Krapez, C. Gruss, R. Huttner, F. Lepoutre, L. Legrandjacques, La camera photothermique partie I : Principe, modelisation, application a la detection dessures. Instrumentation Mesure Metrologie (I2M), 1(2), 9-39 (2001)

[19] S. Moradi, M.H. Kargozarfard, On multiple crack detection in beam structures, Journal of Mechanical Science and Technology, 27(1), 47-55 (2013)

[20] B. Milovanovića and I. Banjad Peĉur, Review of Active IR Thermography for Detection and Characterization of Defects in Reinforced Concrete, Journal of Imaging, 2(2), (2016)

[21] H.S. Carslaw, J.C. Jaeger, *Conduction of Heat in Solids* Clarendon Press, Oxford, 1959.

[22] G. Inglese and R. Olmi, Thermal imaging of time-varying longitudinal defects in the internal coating of a tube, Inverse Problems in Science and Engineering, Inverse Problems in Science and Engineering, 27(4), 439-459 (2019)

[23] J. Gonzales, A. Bedoya, A. Mendioroz and A. Salazar, Measuring the thermal resistance of vertical interfaces separating two different media using infrared thermography, International Journal of Thermal SCiences, 135, 410-416 (2019)

[24] V. Liepa, F. Santosa and M. Vogelius, Crack determination from boundary measurements - Reconstruction using experimental data, Journal of Nondestructive Evaluation, 12(3), 163-174 (1993)

[25] S.C. Jain, Simple Solutions of the Partial Differential Equation for Diffusion (or Heat Conduction), Proceedings of the Royal Society of London. Series A, Mathematical and Physical Sciences, 243(1234), 359-374 (1958)

[26] T.L. Li, D.P. Almond and D.A.S. Rees, Crack imaging by scanning pulsed laser spot thermography, NDT and E International 44, 216-225 (2011)

[27] D.J. Crowther, L.D. Favro, P.K. Kuo and R.L. Thomas, Inverse scattering algorithm applied to infrared thermal wave images *J.Appl.Phys.* 74(9), 5828-5834 (1993)

[28] COMSOL Multiphysics® v. 5.2. www.comsol.com. COMSOL AB, Stockholm, Sweden